Desalination and Water Treatment
www.deswater.com

10 (2009) 181–191

1944-3994 / 1944-3986

The role of reaction time in organic phase on the preparation of thin-film composite nanofiltration (TFC-NF) membrane for dye removal

A. Nora'aini*, A. Norhidayah, A. Jusoh

Department of Science Engineering, Faculty of Science and Technology, Universiti Malaysia Terengganu, 21030, Terengganu, Malaysia
Tel. +60 96683254; Fax +60 96694660; email: noraaini@umt.edu.my

Received 1 September 2008; Accepted in revised form 15 September 2009

ABSTRACT

Dyes are widely used in textile-based industries and inefficiencies in the dying process may result in large amounts of dyestuff being discharged into the wastewater. Membrane separation technology provides relatively high removal for dye wastewater. In this study, local thin-film composite nanofiltration (TFC-NF) membranes for dye removal were fabricated. These membranes were synthesised using an interfacial polymerization technique by reacting *m*-phenylene diamine (MPD) (2.0% w/w) in an aqueous solution and trimesoyl chloride (TMC) (0.2% w/w) in an organic solution. The role of reaction time (5 s, 10 s, 15 s, 20 s, 30 s, 45 s and 60 s) in organic phase on the morphologies, structural details and performances were examined. Membranes were characterized in terms of permeability coefficient, separation of charged solute, membrane structural details and membrane morphology. All fabricated membrane characteristics were in the range of nanofiltration (NF) membranes. The membrane that was prepared with the reaction time 30 s in organic phase (TFC-NF-R30) revealed the highest perm-selective performance due to the trade-off between rejection (87%) and flux (8.65×10^{-6} m^3/m^2s) of charged solute. The membrane was further analysed for the application of dye removals with three representative dyes (Reactive Black 5, Reactive Orange 16 and Acid Yellow 17). The perm-selective TFC-NF-R30 membrane showed a good quality of permeate with dye removal was up to 97%. Moreover, the fluxes ($1.9–11.4\times10^{-6}$ m^3/m^2s) were comparable to those observed with commercial membranes. These findings provide an encouraging platform for applying membrane technology in treating dye wastewater.

Keywords: Dye removal; Nanofiltration; Reaction time; Thin-film composite

1. Introduction

A central breakthrough of membrane application was accomplished by the development of a thin-film composite (TFC) membrane. The term thin-film composite refers to an extremely active thin layer or solute-rejecting dense layer separated from a microporous support layer. The abilities to selectively separate materials are performed at this active thin layer. A microporous support layer presents a mechanical strength and it is highly permeable. The requirements for practical composite membranes are growing year by year. It is due to the desired advantages of TFC membranes such as high water permeability whilst maintaining a great solute rejection behavior. Besides, this membrane has been widely utilized for the production of ultra-pure water, wastewater treatment and recovery of valuable materials [1]. Interfacial polymerization (IP) is one of the established techniques to prepare the TFC membrane. An IP technique is based on the polymerisation reaction which takes place at the interface between

* Corresponding author.

Presented at EuroMed 2008, Desalination for Clean Water and Energy Cooperation among Mediterranean Countries of Europe and the MENA Region, 9–13 November 2008, King Hussein Bin Talal Convention Center, Dead Sea, Jordan.

two monomer solutions (aqueous and organic phase) which are immiscible to each other. The monomers diffuse to the interface where an IP reaction produces an ultra thin-film. Usually, the reaction is very fast, and subsequently the formation of this thin film restrains further reaction [2]. Most of the materials utilized for the polymerisation are reactive amino compound monomers (aqueous phase) and cross-linking agents (organic phase). An aqueous solution containing at least one polyfunctional, water-soluble compound bearing a total of at least two reactive amine groups was prepared. Uemura et al. [3] mentioned that a total of two to four reactive amine groups is most preferable due to the availability of the starting compound and the convenience of handling. Piperazine (primary diamine) and *m*-phenylene diamine (MPD) (secondary diamine) are well-known monomers for aqueous phase. In organic solution, a cross-linking agent may be utilized from essentially polyfunctional, aromatic or cycloaliphatic acyl halides or a mixture of such acyl halides [4]. These compounds have at least three functional groups. Wrasidlo [5] explained that the aromatic acyl halide is preferable because it appears to generate an ultra-thin film that has excellent salt-rejection capabilities. The cross-linking agent should have the superior tendency to react with two reactive amine groups from different polymer chains to achieve the desired cross-linking. Halide can be bromide or chloride.

Conventionally, trimesoyl chloride (TMC), a mixture of trimesoyl chloride and isophthaloyl chloride or terephthaloyl chloride are particularly used as cross-linking agents. Fibiger et al. [6] suggested that the acyl halide should be present in organic solution in a weight percent of 0.06–0.3. The acyl halide should be dissolved in aliphatic solvents (such as pentanes, hexanes, heptanes or octanes) that are not very soluble or immiscible with water. The selection of monomers for aqueous phase and organic phase should be carefully chosen to attain excellent salt rejection and flux characteristics. For the present research, MPD was selected as a polyfunctional reactive amine (in aqueous phase) and TMC as a cross-linking agent (in organic phase). During IP technique, the diffusion of MPD and TMC influenced the polymerisation reaction of amine and chloride acid occurring on the organic side of the aqueous–ogranic interface [7]. Aromatic polyamide is a cross-linked reaction product forming an active ultra-thin layer. In Fig. 1, an aromatic polyamide structure comprises the cross-linked network structure and linear hydrophilic structure. A network chain branching structure, formed by cross-linking reaction of another diamine molecule with terminal acid chloride group of TMC via amide linkage (–CO–NH), increases the membrane rejection at the expense of some flux. A formation of free pendant carboxylic acid structure created by hydrolysis reaction, may also partially contribute to the enhancement of membrane flux [8]. Kwak mentioned that the *meta* positioned (MPD/TMC) aromatic polyamide was suggested to give a better water flux and salt rejection [9].

Extensive literature and patents are concerned with the developing of the active layer membranes that are an extremely ultra-thin and dense. Several parameters have been optimized in order to produce a high-performance TFC membrane, such as kinetic control, material selection and preparation condition [10]. One of the imperative keys of the preparation condition parameters is reaction time in the organic phase. Kim and co-workers [11] studied the effect of polymerisation time (1–5 min with an increment of 1 min) on membrane performances. The salt rejection and volume flux of coated membranes leveled off when the polymerisation time was longer than 1.5 min [11]. Du et al. [12] prepared the composite membrane via interfacially-polymerised of *p*-xyleyne dichloride (XDC) and poly(N,N-dimethylaminoethyl methacrylate) (PDMAEMA). They mentioned that the degree of cross-linking increases with the reaction time. The network structure of PDMAEMA becomes more rigid as the reaction time increases, and the mobility of the polymer chain segments decreases. As a result, the gas permeance through the membrane decreases and the selectivity increases. Verissimo et al. [13] proposed that the reaction period of time should not be too short.

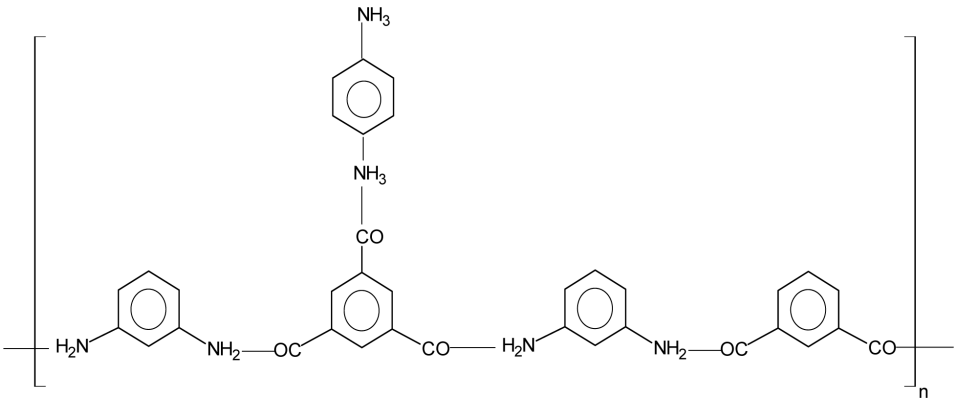

Fig. 1. Chemical structure of aromatic polyamide membrane [12].

Hence, at least 1 min reaction time is needed to get the accurate amount of TMC for the formation of the best separation layer. In order to achieve a great rejection of sodium chloride (99%), the membrane should react with TMC within 2 min [13].

The main goal of the present study is to evaluate the influence of reaction time on the preparation of high perm-selective TFC-NF membrane for dye removal. NF membrane has been proved to be possibly applied for the treatment of solution, with highly concentrated and complex solutions [14]. Koyuncu studied the separation of reactive dye/salt mixtures by employing thin-film nanofiltration membranes. He revealed that the retentions of reactive dye are greater than 99% and the permeates were almost colourless [15]. The performance of perm-selective TFC-NF membranes will be further evaluated at considered low operating pressure (less than 10 bar) with representative dyes of textile-based wastewater. The purpose of the experiment is to evaluate the effectiveness of TFC-NF membranes in treating wastewater containing dyes.

2. Methodology

2.1. Preparation of membrane samples and permeation experiment

2.1.1. Chemicals

All chemicals were of analytical grade with a purity over 99%. Polysulfone (PSf) Udel-P1700 was supplied by Amoco Chemicals. TMC and MPD, Reactive Black 5 (RB5), Reactive Orange 16 (RO16) and Acid yellow 17 (Ay17) were obtained from Sigma Aldrich.

2.1.2. Preparation of a UF membrane

A UF membrane was used as a UF membrane support layer of a composite membrane. A dope composition of the UF membrane consists of PSF (15%w/w) and DMF (85% w/w). The membrane was prepared via a simple dry–wet phase inversion and cast using a semi-automated electrical casting machine. A polymer solution was poured onto a glass plate and spread with a casting knife at an approximately constant shear rate of 160 s^{-1}. The nascent membrane was evaporated at room temperature for 10 s. Then the membrane was immersed in a water coagulation bath overnight. After the immersion step, the membrane was solvent-exchanged in methanol (8 h) to ensure the excess solvent and water-soluble polymer was totally removed. Finally, the membrane was dried at room temperature.

2.1.3. Preparation of a thin-film composite (TFC) membrane

TFC membranes were developed by IP technique. MPD was employed in an aqueous solution with the concentration of MPD being 2.0% w/w. The concentration of TMC in *n*-hexane (organic solution) was 0.2% w/w with the ratio of TMC to MPD 1:10. The TFC membrane prepared simply and efficiently by a general series of steps comprising (1) placing the UF membrane support layer in the solution for 2 min to permit complete saturation of the UF membranes with MPD solution (aqueous phase), (2) removing of excess MPD by pressing softly the membrane without damaging the membrane surface, (3) immersing the membrane coated with MPD into the solvent solution of TMC (organic phase) for different periods of time (5 s:TFC-NF-R5, 10 s: TFC-NF-R10, 15 s: TFC-NF-R15, 20 s: TFC-NF-R20, 30 s: TFC-NF-R30, 45 s: TFC-NF-R45 and 60 s: TFC-NF-R60), and (4) drying the membrane at ambient temperature. The membranes were characterized in terms of permeability coefficient (P_m), membrane morphology and membrane structural details. The permeation experiment was performed using dead-end cell filtration model Sterlitech HP4750 Stirred Cell with 300 mL processing permeate, effective permeation membrane area of 14.6 cm^2, cell diameter 5.1 cm and cell height 22.4 cm. The operating pressure of pure water permeation experiment was from 1 to 7 bar. The cell was pressurized by using the compressed nitrogen-free oxygen whereby the applied pressures were controlled by the cylinder regulator. Sodium chloride (NaCl 0.01 M) solution was prepared to investigate the separation performance of charged solutes at operating pressure 5 bar. The permeate and feed concentrations of NaCl were measured using a conductivity meter (Hanna Instruments model HI8633). The volume flux ($J_{v,i}$), observed rejection ($R_{i,obs}$) and real rejection ($R_{i,real}$) were calculated using Eqs. (1)–(3).

$$J_{i,v} = V_i / At \tag{1}$$

$$R_{i,obs} = 1 - C_{i,p} / C_{i,r} \tag{2}$$

$$R_{i,real} = 1 - C_{i,p} / C_{i,w} \tag{3}$$

The membrane structural details were estimated by employing sodium chloride rejection measurement in conjuction with theoretical approaches. The steric hindrance pore (SHP) model and Teorell-Meyers Sievers (TMS) model were employed to deduce the pore size (r_p), ratio of thickness to porosity ($\Delta x/A_k$) and ratio of charge density to bulk concentration ($\zeta = X_d/C_b$) [16]. Scanning electron microscopy (SEM model P/N HP4750) was employed to analyse the membrane cross-section and membrane surface. For this purpose, the samples of membranes were cryogenically fractured in liquid nitrogen. The membrane specimens were then subsequently coated with gold by using an automatic coater (model JFC 1600). After sputtering the parts with gold, they were transferred to the microscope and the cross-section and surface were observed under magnifications of 1500× and 500×, respectively.

2.1.4. Membrane separation performances in treating wastewater containing dye

A high performance of the perm-selective TFC-NF membrane was further analysed by examining the separation performance of artificial dye wastewater. Fig. 2 shows the chemical structure of three representative dyes — RB5, RO16 and Ay17 that are widely used in the dye-based industry. Dye solutions were prepared at a concentration of 100 mg/L. All samples were tested by applying UV spectrophotometer at wavelengths 597 nm, 618 nm and 493 nm for RB5, RO16 and Ay17, respectively.

2.2. Characterisation of membrane using establish mathematical models

2.2.1. Steric hindrance pore (SHP) model

An ionic flux can be described by a common assumption of the extended Nernst–Planck equation. Indeed, some authors have found the steric hindrance effects by rearranging the extended Nernst–Planck equation in order to estimate the ion flux inside a charged NF membrane as expressed in Eq. (4). H_F and H_D parameters are for steric hindrance and frictional forces that impede convective and diffusive transport, respectively, and are expressed by the SHP models as in Eqs. (5)–(10).

$$J_i = v_i k_i \left[H_{F,i} u_x c - H_{D,i} D_i \left(\frac{dc}{dx} + c \frac{z_i F d\phi}{RT dx} \right) \right] \tag{4}$$

$$\sigma = 1 - H_F S_F \tag{5}$$

$$P_s = H_D S_D D_S \left(A_K / \Delta x \right) \tag{6}$$

$$H_D = 1 \tag{7}$$

$$H_F = 1 + \frac{16}{9}\eta^2 \tag{8}$$

$$S_F = (1-\eta)^2 \left[2 - (1-\eta)^2 \right] \tag{9}$$

$$S_D = (1-\eta)^2 \tag{10}$$

2.2.2. Teorell-Meyer-Sievers (TMS) model

TMS model is a rigorous approach to describe the membrane electrical properties in terms of effective charge density, X_d and electrostatic effects, ζ. This model has been extensively used to explain the transport mechanism in NF membranes considering the electrostatic effects for the permeation of electrolyte (NaCl). The TMS model assumed a uniform radial distribution of fixed charges and mobile species. Bowen et al. [17] explained that these assumptions are suitable at low concentrations and in pores smaller than 2 nm. The modelling results clearly show that the electrolyte ions have a larger size than the membrane pore radius. The TMS model is represented by Eq. (11) and Eq. (12).

$$\sigma_{salt} = 1 - \frac{2}{(2\alpha - 1)\xi + (\xi^2 + 4)^{1/2}} \tag{11}$$

$$P_{salt} = D_S (1 - \sigma_{salt}) \left(\frac{A_K}{\Delta x} \right) \tag{12}$$

3. Results and discussion

3.1. UF membrane

A UF membrane was used as a microporous support for the thin barrier layer of the composite membrane. This membrane was characterized by means of permeability coefficient (P_m) and morphology. The characteristics of this membrane play a crucial role in determining the total resistance to transport via the membrane and the separation behaviour. The P_m of the UF membrane is

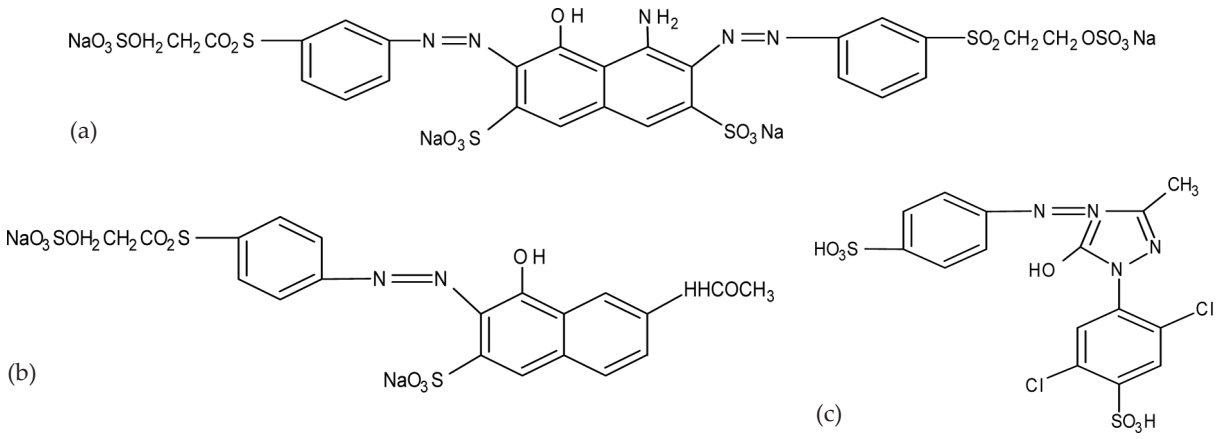

Fig. 2. Chemical structure (a) Reactive Black 5 (MW = 982 g/mole, r_p = 0.97 nm), (b) Reactive Orange 16 (MW = 616 g/mole, r_p = 0.54 nm), and (c) Acid Yellow 17 (MW = 551 g/mole, r_p = 0.52 nm).

about 8.492×10^{-6} m^3/m^2.s.bar [18]. Membrane morphology (surface and cross-section) plays a significant effect in determining the membrane separation performance. The membrane cross-section (magnification of 1500×) and membrane surface (magnification of 500×) were analysed using SEM. As illustrated in Fig. 3, the UF membrane comprises a skin layer that is well-developed and supported by a porous support layer with large finger-like porous structures. The separation behaviour occurred at the skin (active) layer of the membrane. The bottom layer, which is the support layer, acts as the mechanical strength of the membrane. Membrane pores decreased in diameter from the bottom to the top surface of the membrane. The membrane skin layer shows a rough surface and contains superficial craters, nodules and scratches.

Prior to the separation performance, the UF membrane was tested with charged solute (NaCl 0.1 M). The volume flux of the UF membrane was about 21.08×10^{-6} m^3/m^2.s. It should be ten times higher than the coated layer (thin film). This ensures that more than 90% of the resistance to flow lies within the selective thin film [18]. As well as having a higher flux, the UF membrane also gave a high rejection (45.16%). This value is contributed to by a very finely microporous UF membrane. The pores must be small enough to support the selective thin film under high pressures, and must also be close together so the permeating components do not take a long tortuous path to reach the pore. In addition, the rejection value is acceptable and has a minimum resistance to the solutes that pass through it. Thus, the developed membrane fulfilled the criteria as a microporus membrane support layer.

3.2. Membrane characterization

Seven TFC-NF membrane samples were prepared with various reaction periods of time in an aqueous phase. The reaction was conducted at pre-determined reaction times 5 s, 10 s, 15 s, 30 s, 45 s and 60 s coded as TFC-NF-R5, TFC-NF-R10, TFC-NF-R15, TFC-NF-R20, TFC-NF-R30, TFC-NF-R45 and TFC-NF-R60, respectively. Membranes were characterized in terms of P_m, membrane morphology and membrane structural details as shown in Table 1. Fig. 4 shows the P_m of TFC-NF membranes. Results expose that the P_m of TFC-NF membranes are lower as compared to the P_m of the UF membrane. It could be suggested that the lower P_m of the TFC membranes is a result of an IP process. This process tends the membrane to make structural changes from an asymmetric structure to a composite structure. In addition, the IP process also leads to a formation of dense thin layer at the skin membrane, providing an additional flow resistance. TFC-NF membranes were synthesised by reacting MPD in an aqueous solution and TMC in organic solution. The TFC-NF-30 reveals the highest value of P_m and TFC-

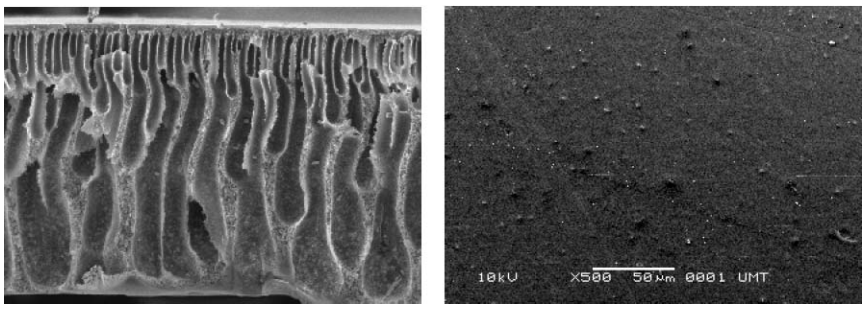

Fig. 3. SEM micrograph on the UF membrane support layer (a) membrane cross-section (b) membrane surface.

Table 1
Permeability coefficient, flux and rejection of charge solute, and structural details of TFC NF membranes at applied pressure 5 bar

Membrane ID	P_m [10^{-6}] m^3/m^2.s.bar	J_v [10^{-6}] m^3/m^2.s.	R [%]	rp [10^{-9}] m	Δ_x/A_k [10^{-4}] m	X_d mol/m^3	ξ
TFC-NF-R5	2.023	9.589	78.53	1.872	0.590	–0.366	–3.658
TFC-NF-R10	1.965	8.154	80.14	1.810	6.681	–0.425	–4.254
TFC-NF-R15	1.919	7.821	85.30	1.627	6.159	–0.750	–7.496
TFC-NF-R20	1.886	6.969	88.63	1.520	6.370	–1.202	–12.023
TFC-NF-R30	2.217	8.654	86.88	1.575	5.356	–0.925	–9.245
TFC-NF-R45	1.072	4.979	80.41	1.800	10.873	–0.437	–4.367
TFC-NF-R60	0.946	4.419	83.02	1.705	11.518	–0.573	–5.729

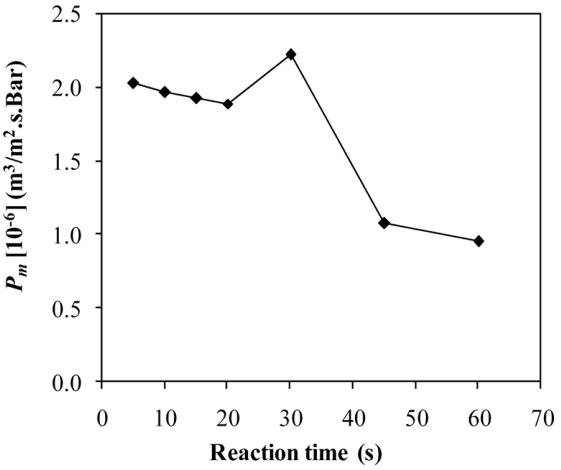

Fig. 4. The values of Pm with different reaction times.

NF-R60 exposes the lowest value of P_m. Small reductions of P_m can be achieved at shorter reaction times (5–20 s). However, a moderate increase of P_m was noticed at the reaction time 30 s (TFC-NF-R30). It postulates that the TFC-NF-R30 probably contains macrovoid structures at the bottom layer of the membrane. P_m severely dropped at the reaction time of 45 s. Besides, the P_m of TFC-NF-R60 gradually decreased due to the thicker ultra-thin layer which resulted in increasing the film growth rate. The P_m of membranes is in the range of NF membranes, from fluxes similar to those typical of UF to reverse osmosis membranes [17]. Figs. 5 and 6 show the SEM micrographs for cross-section and surface of the TFC-NF membranes. It can be clearly seen that all membranes consist of a typically composite structure. However, TFC-NF-R30 displays a transition structure from a typical asymmetric structure to a composite structure. An asymmetric struc-

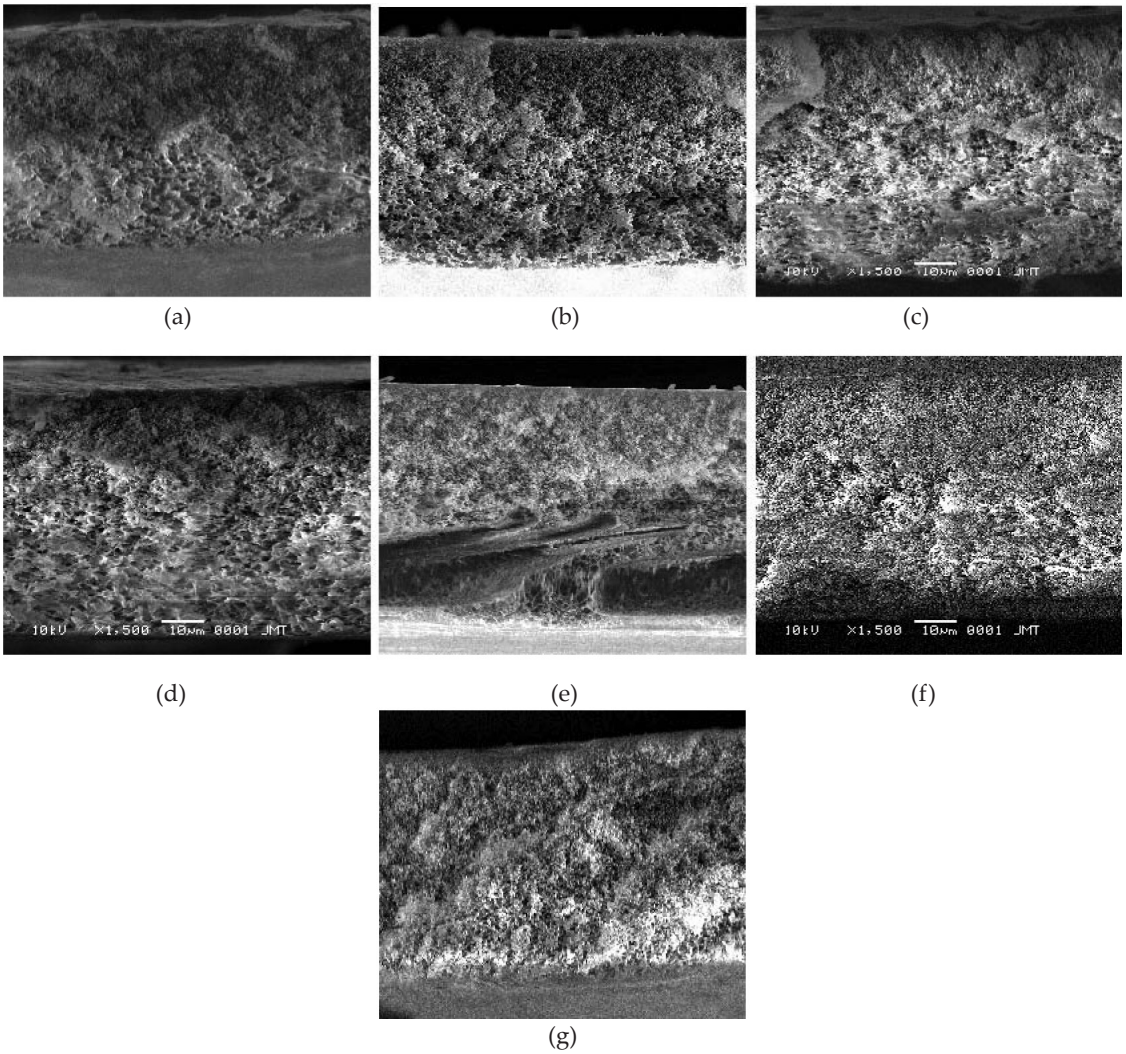

Fig. 5. SEM micrographs of membrane cross-section at magnification of 1500× (a) TFCNF-R5, (b) TFC-NF-R10, (c) TFC-NF-R15, (d) TFC-NF-R20, (e) TFC-NF-R30, (f) TFC-NF-R45, and (g) TFC-NF-R60.

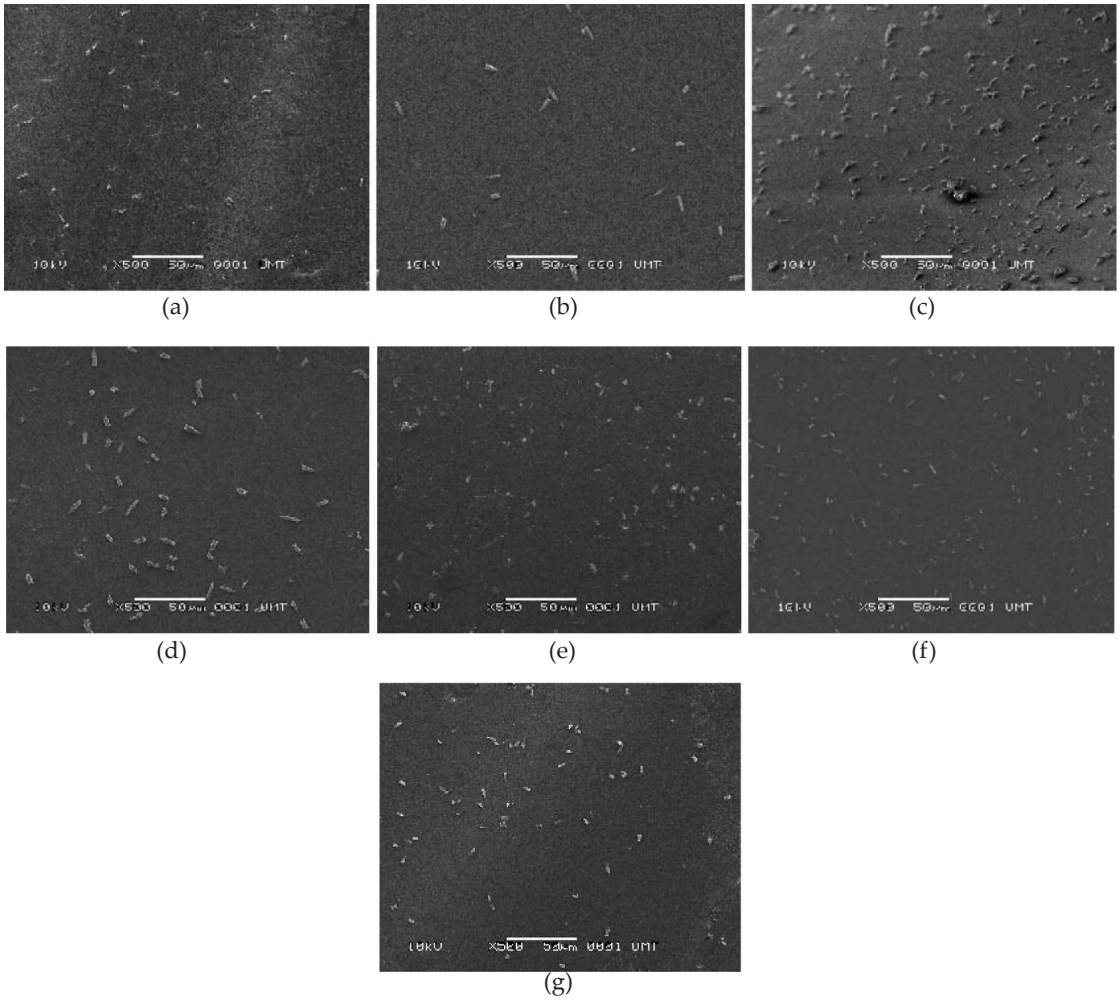

Fig. 6. SEM micrographs of membrane surface at magnification of 500x (a) TFC-NFR5, (b) TFC-NF-R10, (c) TFC-NF-R15, (d) TFC-NF-R20, (e) TFC-NF-R30, (f) TFC-NF-R45, and (g) TFC-NF-R60.

ture can be described by the presence of macrovoid at the bottom layer, which leads to a high flux. The composite structure can be elaborated by the presence of a thicker, bulky and distinctive solid layer to be coated on the skin layer. This layer is responsible for a great rejection performance. In Fig. 6, the micrographs of membrane surface structures demonstrate that all membranes comprise the ridge and valley structure. This structure will act as the active functional site on the membrane surface which tends to increase the membrane rejection. Additionally, a longer reaction time in the organic phase forms a rougher membrane surface, due to the incorporation of TMC as well as hydrolysis process.

The permeation experiment of NaCl was performed at an applied pressure of 5 bar. The fluxes and rejection with different reaction periods of time are presented in Fig. 7. As can be seen, it is very clear that the rejection increased whereas the flux decreased with increasing of reaction times from 5 s to 20 s. The reaction time influences an extent of polymerisation as the reaction is mainly controlled by the diffusion of MPD through interfacially-produced polyamide film and the diffusion of TMC in the organic phase. Consequently, it is realistic to mention that a shorter reaction time would produce a thin and loose polyamide skin layer. In addition, the extended degree of cross-linking is comparatively lower at shorter reaction times, leading to a lower rejection. On the contrary, the rejection and flux show an inverse trend for the reaction time of 30 s. The rejection was slightly reduced and the flux was sharply increased. It illustrates that the flux seems to reach its limit at 30 s reaction time. Then, the rejection continuously reduced at longer reaction times (45 s and 60 s). However, the flux drastically reduced for the reaction time 45 s and then gradually decreased for the reaction time 60 s. This might be due to the extensive cross-linking and film growth that tends to give a lower flux at longer reaction times. As a result, a thicker and denser polyamide skin layer was formed. The highest

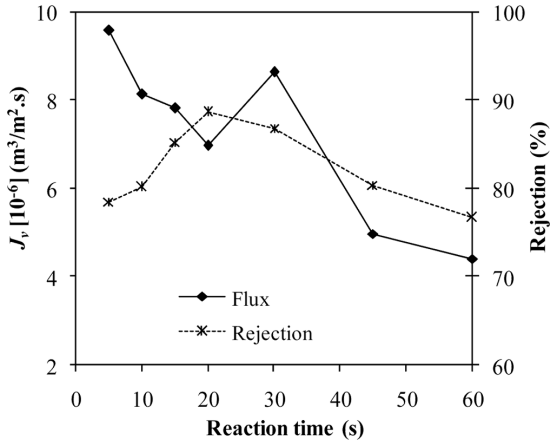

Fig. 7. Fluxes and rejections of sodium chloride with different reaction times.

rejection was obtained at the reaction time 20 s. However, this membrane has a moderately low flux. Regarding the flux, the membranes that reacted within 30 s revealed the highest flux and moderate rejection, respectively. In this particular case, it is reasonable to claim that an optimum reaction time of TFC membrane is 30 s due to a high perm-selectivity property of the membrane.

Based on the flux and rejection of NaCl, the membrane structural details in terms of membrane pore size (r_p), ratio of thickness to porosity ($\Delta x/A_k$) and membrane charge density (X_d) can be approximated. The r_p, and $\Delta x/A_k$ are deduced by employing the SHP model and X_d from TMS model [16]. In this study, the modeling results demonstrate that all membrane pore sizes are in the range of a typical pore size of 29 commercial NF membranes as shown in Table 2 [17]. It was revealed that the TFC-NF-R20 has the smallest pore size which provides a great resistance of fluid and solutes to pass through the membrane pores. The membrane pore sizes were gradually decreased from 5 s to 20 s reaction time.

A shorter reaction time would not allow a sufficient time of acid chloride (TMC) to polymerize the diamine of MPD. It is reasonable to explain that lower reaction time forms a larger pore size which leads to higher permeation of water and salt. Nevertheless, after the reaction time 20 s, the pore sizes of membranes become larger. The pore loosening occurs at the reaction times longer than 20 s. These membranes exert to be less resistance to water flow, resulting to the enhancement of fluxes. During an interfacial polymerization process, acid hydrochloric is produced as a by product. It hydrolyzes the TMC to carboxylic group (–COOH). However, the longer the reaction times produce the greater content of –COOH. It tends to the higher ratio of hydrophilic groups, resulting to the exceeding water uptake.

Table 2
Summary of the characteristics of 29 commercial NF membranes [19]

Parameters	Maximum	Minimum	Average
r_p (nm)	1.80	0.39	1.59
ξ-ve	44.5	1.5	9.2
Δ_x/A_k (mm)	16.9	0.66	4.8

Further explanations focused on the other membrane structural details such as ratio of the membrane thickness to membrane porosity ($\Delta x/A_k$) and membrane surface charge (X_d). When the reaction times increased from 5 s to 20 s, only small change was observed. This trend was favoured to a small alteration of the membrane pore size, which reflected the membrane porosity. The shorter reaction times produced a thin and loose polyamide skin layer. In addition, at these ranges of reaction times, acid chloride (TMC) had no sufficient time to extend the polymerization process of diamine (MPD). As a result, it contributed to a larger porosity and thin polyamide skin layer. At the reaction time 30 s, the value of $\Delta x/A_k$ was slightly decreased. For the reaction time that longer than 30 s, the values of $\Delta x/A_k$ were gradually decreased. Increase in reaction times would result in increase of an extent of polymerization process which leads to the increment of film growth, thus lower fluxes. The influence of reaction times in organic phase on the membrane electrostatic (X_d and ξ) structural details were also evaluated. In Fig. 8, it is demonstrated that the polymeric membrane is negatively charged under normal circumstances. The TFC-NFR20 provides the highest value of X_d tends to have the greatest rejection. However, the lowest value of X_d (TFC-NFR60) allows the smallest rejection. This is due to the assumption that a lower value of X_d exhibits a small volume of charge on the membrane surface. It allows a weak repulsion between the membrane surface charge and a chloride ion (Cl^-), thus a lower rejection. The shorter reaction times from 5 s to 20 s expose a gradually increased of X_d. However, the values of X_d were decreased when the reaction times were longer than 20 s.

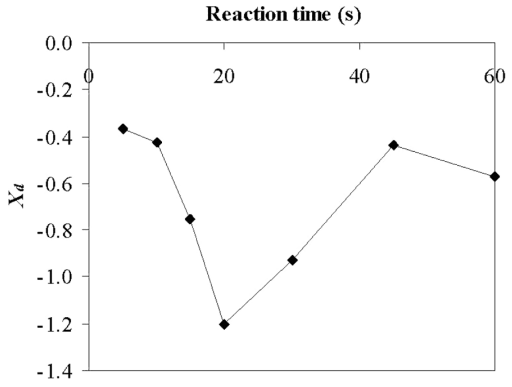

Fig. 8. Membrane charge density with different reaction times.

3.3. Membrane performance in treating wastewater containing dye

The reaction time 30 s (TFC-NFR30) was selected as an optimum period to polymerize the coating layer of MPD on the UF membrane surface. A selection was made based on the trade off between flux and rejection of sodium chloride (high perm-selective TFC-NF membrane), as shown in Fig. 7. The goal of the following research is to obtain a general understanding of a possibility of the membrane to separate dye-based wastewater. Based on this purpose, certain dyes were selected such as RB 5 (r_s = 0.665 nm), R016 (r_s = 0.543 nm) and Ay 17 (r_s = 0.516 nm). The operating pressure was from 1 to 7 bar. Fig. 10 plots the flux of three various dye solutions that were treated using TFC-NFR30. It can be seen that as the pressure increases, the fluxes for each dye also increase. The fluxes of dye solutions penetrated across the membrane per unit time and changed according to the dye solution. One of the factors that influence the volume flux is the diffusivity of dye. It can be estimated by employing the Stokes–Einstein equation ($D = kT/6\pi\mu rs$). The diffusivities of RB 5, RO 16 and AY 17 are 4.11×10^{-10} m/s, 4.83×10^{-10} m/s and 5.13×10^{-10} m/s, respectively. AY 17 shows the highest diffusivity of dye, leading to the greatest mobility. As a result, the highest volume flux and the lowest separation behaviour can be achieved. When the applied pressures were lower than 5 bar, the fluxes were leveled off. It seems that at applied pressure 5 bar, TFC-NFR30 approached the limiting flux. The flux behaviours are in good agreement with the Darcy's law, whereas flux is directly proportional to the applied pressure $J = K\,\Delta P$, and constant K relates to the membrane structure and viscosity of permeating fluid.

Fig. 9 clearly shows that a high perm-selective TFC-NF membrane (TFC-NFR30) rejected more than 80% of dyes. At applied pressure of 5 bar, the highest rejection of dyes were obtained — about 97%, 93% and 92% for RB5, RO16 and AY17, respectively. As expected, RB5 has the largest size than RO 16 and AY 17, thus the highest rejection. A comparison was made between r_p of TFC-NFR30 and solute radius of dyes in order to explain the dye rejection. In this case, the solute radius of dyes is lower than TFC-NFR30 pore size. Interestingly, the rejections show the higher abilities. The probable reason is that the molecular sieve mechanism alone is insufficient to elaborate the separation performance of dyes. TFC-NFR30 has negatively charged membrane surface (X_d = -0.925) due to the presence of carboxylic substitute at the heterocyclic aromatic rings. Dyes contain the functional groups which substitute at the heterocyclic aromatic rings. Therefore, the charged exclusion (Donnan effect) takes place in the interaction between dyes and fixed electric charge density that attached to the membrane surface. It appears that the electrostatic property of dyes can allow the higher rejection of dyes. This indicates that the electrostatic interaction between the membrane surface and the dye particles can be observed as other factor that significantly affects the effectiveness of the membrane separation process.

Fig. 10 illustrates the rejection ability for TFC-NFR30 in treating the artificial wastewater containing dyes. Similar to the flux, the rejection gradually increased at lower operating pressures (15 bar) and then, leveled-off at the extended operating pressure (6–7 bar). This phenomenon might be explained by the influence of concentration polarization at the feed membrane interface. The presence of concentration polarization tends to build up solute particles over the membrane surface. Thus, an osmotic pressure near the membrane surface increased due to the convective transport through the membrane. It led to enhancing the solute permeation. At the same time, it tends to slightly decrease the dye rejection. After the membrane separation process, the membrane surfaces were covered by the deposited dyes. It revealed that the dye tended to strongly attach to the membrane surface because the reactive dyes have amino, sulphonic and

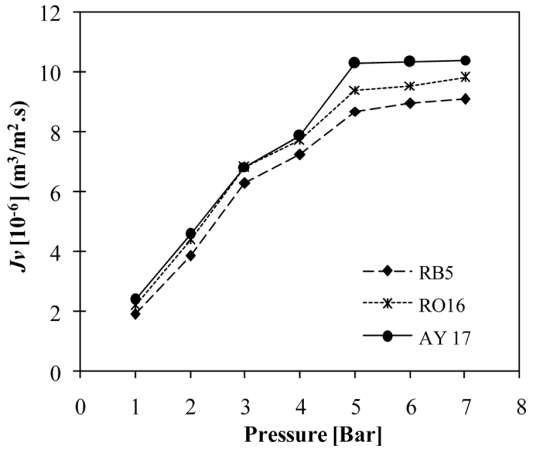

Fig. 9. Flux of RB 5, RO 16 and AY 17 by using TFC-NF-R30.

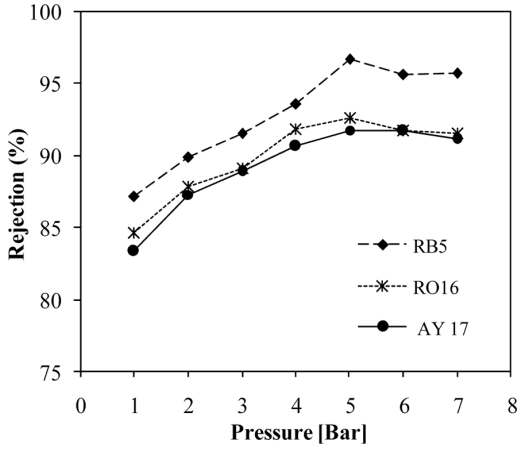

Fig. 10. Rejection of RB 5, RO 16 and AY 17 by using TFC-NF-R30.

hydroxyl groups as substitutes bound to the aromatic rings which describe the phenomenon of fouling effect in the membrane separation process.

4. Conclusion

TFC membranes were successfully developed via interfacial polymerization with respected to different reaction times. The membrane characteristics were postulated to be in the range of the NF membrane. Based on the trade off between flux and rejection of sodium chloride, the membrane prepared under the reaction time in organic phase within 30 s (TFC-NFR30) can be claimed as an optimum period for the polymerization process. A high perm-selective TFC-NFR30 membrane was further analyzed in treating artificial wastewater containing dyes. The results show that the TFC-NR30 has a reasonable flux and good permeate quality in removing dyes from wastewater. During the separation process, the Donnan and steric exclusion play a crucial role in the separation mechanism. The rejection of dyes decreased in the sequence of RB 5 > RO 16 > Ay 17. The findings of this research show that the TFC membranes seem to be a possible and a realistic technology for the treatment of wastewater containing dyes.

Acknowledgement

The authors wish to express their sincere gratitude to the Ministry of Science, Technology and Innovation, Malaysia, for the financial support, and also Engineering Science Department, Institute Oceanography, Universiti Malaysia Terengganu and Mrs. Sofiah Hamzah for their help and support.

Symbols

A_K — Membrane porosity
A — Membrane area, m
c — Concentration, mol/m^3
D_i — Diffusivity of ion i in free solution, m^2/s
Ds — Solute diffusivity for neutral molecule or generalized diffusivity for 1-1 type of electrolyte define as $Ds = 2(D_1/D_2)/(D_1 + D_2)$, m^2/s
F — Faraday constant, 96487 C/mol
$H_P H_D$ — Steric parameters related to wall correction factors under diffusion and convection conditions, respectively
$J_{v,i}$ — Average solute volume over membrane surface, m/s
K_i — Average distribution coefficient of ion, i by the electrostatics effect
P — Applied pressure, bar
P_s — Solute permeability, m/s
$R_{i,\,obs}$ — Observe rejection of component i, %
$R_{i,real}$ — Real rejection of component i, %
r_p — Pore radius,m
r_s — Solute radius, m
$S_P S_D$ — Distribution coefficient of solute by steric hindrance effect under diffusion and convection condition, respectively
t — Time, s
X_d — Effective membrane charge density, mol/m^3
Z_i — Valence of ion

Greek

η — Ratio of solute radius to membrane pore radius
σ — Reflection coefficient, %
Δx — Effective membrane thickness, m
ξ — Ratio of fixed charge density to salt concentration

References

[1] H. Hachisuka and K. Ikeda, Composite reverse osmosis membrane having a separation layer with polyvinyl alcohol coating and method of reverse osmosis treatment of water using the same. US Patent 6177011, 2001.
[2] A.P. Korikoz, P.B. Kosaraju and K.K. Sirkar, Interfacially polymerized hydrophilic microporous thin film composite membranes on porous propylene hallow fibers and flats films. J. Membr. Sci., 279 (2006) 588–600.
[3] T. Uemura, Y. Himeshima and M. Kurihara, Interfacially synthesized reverse osmosis membrane. US Patent 4 761 234, 1988.
[4] J.E. Tomaschke, Amine monomers and their use in preparing interfacially synthesized polyamide membranes for reverse osmosis and nanofiltration. US Patent 5 922 203, 1999.
[5] W.J. Wrasidlo, Composite semipermeable membrane made form polyethlenimine. US Patent 3 951 815, 2006.
[6] R.F. Fibiger, J.Y. Koo, D.J. Firgach, R.J. Peterson, D.L. Schmidt, R.A. Wessling and T.F. Stocker, Novel polyamide reverse osmosis membranes, US patent 4 859 384, 1998.
[7] G.Y. Chai and W.B. Kranzi, Formation and characterization of polyamide membranes via interfacial polymerization. J. Membr. Sci., 93 (1994) 175–192.
[8] A.P. Rao, S.V. Joshi, J.J. Trivedi, C.V. Devmurari and V.J. Shah, Structure-performance correlation polyamide thin film composite membranes: Effect of coating conditions on thin film formation. J. Membr. Sci., 211 (2003) 13–24.
[9] S.Y. Kwak, S.G. Jung, Y.S. Yoon and D.W. Ihm, Details of surface features in aromatic polyamide reverse osmosis membrane characterized by scanning electron and atomic force microscopy. J. Polymer Sci. B: Polymer Physics, 37 (1999) 1429–1440.
[10] A.L. Ahmad and B.S. Ooi, Properties-performance of thin film composites membrane: Study on trimesoyl chloride content and polymerization time. J. Membr. Sci., 225 (2005) 67–77.
[11] C.K. Kim, J.H. Kin, I.J. Roh and J.J. Kim, The changes of membrane performance with polyamide molecular structure in the reveres osmosis process. J. Membr. Sci., 165 (2000) 189–199.
[12] R. Du, A. Chakma and X. Feng, Interfacially formed (N,N-dimethylaminoethylmethacrylate)/polysulfone composite membranes for CO_2/N separation. J. Membr. Sci., 290 (2007) 19–28.
[13] S. Verissimo, K.V. Peinamann and J. Bordado, Influence of the diamine structure on the nanofiltration performance, surface morphology and structure charge of the composite polyamide membranes. J. Membr. Sci., 279 (2006) 266–275.
[14] C. Allegre, P. Moulin, M. Maissue and F. Charbit, Treatment and reuse of reactive dyeing effluent. J. Membr. Sci., 269 (2006) 15–34.
[15] I. Koyuncu, Reactive dye removal in dye/salt mixture by nanofiltration membranes containing vinylsulphone dyes: Effects of

feed concentration and cross flow velocity. Desalination, 143 (2001) 243–253.
[16] A.R. Hassan, A. Nora'aini, A. Norhidayah and A.F. Ismail, A theoretical approach on membrane characterization: The deductions of fine structural details of asymmetric nanofiltration membranes. Desalination, 206 (2007) 107–126.
[17] J.R. Bowen, A.W. Mohamad and N. Hilal, Characterization of nanofiltration membranes for predictive purpose-use of salts, uncharged solutes and atomic force microscopy. J. Membr. Sci., 126 (1997) 91–105.
[18] M. Mulder, Basic Principle of Membrane Technology, 2nd ed., Kluwer, 1996.